IL NUOVO CIMENTO **38 C** (2015) 73
DOI 10.1393/ncc/i2015-15073-6

Communications: SIF Congress 2014

Search for extended γ-ray emission around AGN with MAGIC telescopes

P. Da Vela on behalf of the MAGIC Collaboration

INFN, Sezione di Pisa - Pisa, Italy
Dipartimento di Scienze Fisiche, della Terra e dell'Ambiente, Università di Siena
Siena, Italy

received 30 January 2015

Summary. — TeV photons coming from a distant extragalactic source are not able to propagate over large distances because they interact with the extragalactic background light photons producing pairs e^+e^-. These pairs, in turn, interact with the cosmic microwave background via inverse-compton producing a secondary γ-ray emission at lower energies. Extragalactic magnetic fields alter the trajectories of the electron pairs hence the secondary emission can be extended around the TeV sources. This process can be used to constrain the magnetic fields in the inter-galactic medium. We present the study of the emission profile of the blazar Markarian 421 yielding upper limit on the halo flux of the order of 1.5% Crab units in the energy range 300–1300 GeV.

1. – Introduction

Magnetic fields are known to play an important role in a variety of astrophysical objects, from stars to galaxies and galaxy clusters [1]. The strength of the magnetic fields in the astrophysical sources can pe probed using different techinques such us Faraday rotations and Zeeman splitting of atomic lines in the radio band. Besides the measure of the synchrotron emission in the radio band provides us another important tool to estimate the magnetic field. Magnetic fields stregnth in the range 1–100 μG are found in many galaxies [2-5]. Recently, weaker magnetic fields with strength in the range 10^{-8}–10^{-7} G were discovered at the outskirts of galaxy clusters [6, 7].

Although in many cases we know quite well the strength and the structure of the magnetic fields, their origin remains largely unknown. To explain the current magnetic field in the galaxies, amplification mechanisms like the so-called $\alpha - \omega$ dynamo process or compression of turbulent motions of plasma during the galaxy formation are usually invoked. However all these mechanisms are based on the assumption that seed fields

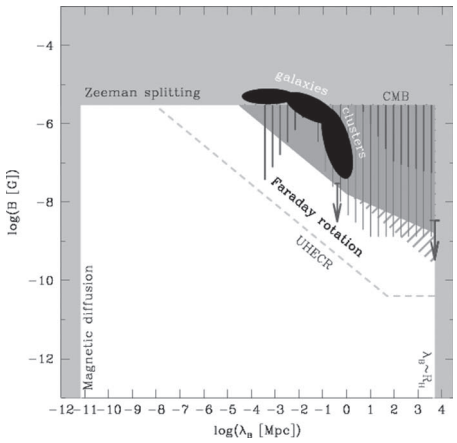

Fig. 1. – Observational limits on IGMF.

were already present and later amplified. The nature of the initial fields for the dynamo or turbulent amplification is not understood.

From the theoretical point of view two main hypotheses on their origin exist: the *astrophysical origin* and the *cosmological origin*. In the *astrophysical origin* hypothesis the seed fields are produced during the epoch of galaxy formation by electrical currents that can have different astrophysical origins or via the so-called Biermann battery effect at the early stages of galaxy formation. Differently, in the *cosmological origin* the seed fields might originate from still earlier epochs of the Universe expansion, down to the cosmological phase transitions or inflation times. For a recent review see, *e.g.*, [8].

The main difference between these two scenarios is in the fact that if we assume cosmological magnetic fields this means that seed fields should be present everywhere the Universe today. In particular the seed fields could be found in the voids of large scale structure, among galaxies and galaxy clusters. On the contrary if we assume an astrophysical origin for the magnetic fields, no magnetic field generation outside galaxies and clusters is expected. Magnetic fields in the voids of large scale structure is expected to be close to zero. To shed some light on the origin of the seed fields, observational measurements in the Inter Galactic Medium (IGM) are needed.

2. – Existing limits on inter-galactic magnetic field

Contrary to the magnetic fields in the galxies and galaxy clusters the Inter-Galactic Magnetic Field (IGMF) has never been detected. Only upper limits, obtained with the cited techniques exist. In this section we present the exisiting limits on IGMF.

In the simplest settings, the IGMF configuration can be characterized by two parameters: the field strength B, and the correlation length λ_B, the scale length within which we can consider the magnetic field uniform and constant. All limits on IGMF derived from the observations can be presented in the so-called exclusion plot (B, λ_B) (fig. 1) as a function of these two parameters.

Magnetic fields in the IGM decay due to magnetic diffusion over a scale length that can be derived using the relation for the diffusive time $\tau_d = 4\pi l^2 \sigma$ where $\sigma \simeq 10^{11}\,\mathrm{s}^{-1}$ is the conductivity of the Universe after recombination. Using the Hubble time T_H in the place of τ_d we get $l_{diff} \simeq 2 \times 10^{13}\,\mathrm{cm}$. Hence the correlation length is limited from below

to $\lambda_B > l_{diff}$. At the same time a reasonable upper bound comes from the size of the visible part of the Universe namely the Hubble radius, $\lambda < R_H$. The limits on λ_B are shown in fig. 1.

2˙1. *Zeeman splitting.* – In vacuum, the electronic energy levels of an atom are independent of its angular momentum vector. A magnetic field removes this degeneracy by picking out a particular direction in space. The energy splitting between neighboring levels ΔE is proportional to the magnetic field B so that once ΔE is measured B can be determined without additional assumption. Zeeman splitting is the most direct method for observing astrophysical magnetic fields. Measuring the Zeeman splitting of the 21 cm hydrogen line in the spectra of distant quasar it was possible to infer the magnetic field in the Milky Way [9] as well as in other galaxies [5]. Measurements of $B \sim \mu G$ in the Milky Way or in other galaxies exclude the possibility to have stronger magnetic field in the IGM. This limit does not depend on the correlation length and in the exclusion plot it is represented by an horizontal line.

2˙2. *Faraday rotation.* – When polarized emission propagates in a region with ionized gas and magnetic field, it undergoes Faraday rotation wherein left and right-circular polarization states travel with different phase velocities. For linearly polarized radiation, this results in a rotation with time (or equivalently path length) of electric field vector by an angle $\phi \propto \lambda^2 B_\parallel n_e D$, where λ is the wavelength of the radiation, $B_\parallel$ is the magnetic field along the line of sight, n_e the density of the thermal electrons along the line of sight and D is the distance to the source. Measuring ϕ and assuming a particular electron density in the IGM it is possible to estimate the IGMF. As we can see in fig. 1 the limits on IGMF computed measuring the Faraday rotation of polarized emission depend on the correlation length λ_B. This is because if $\lambda \ll R_H$ the polarization angle experiences random changes due to the passages of multiple domains of the size of the order of λ_B with coherent magnetic field. This means that ϕ changes proportionally to the sqaure root of the distance ($\phi \propto \sqrt{D\lambda_B}$). Non detection of IGMF due to Faraday rotation implies an upper limit on B which depends proportionally on $\sqrt{\lambda_B}$.

2˙3. *Deflection of ultra high energy cosmic rays.* – Magnetic field in the IGM can be constrained measuring the effect that IGMF has on the trajectories of Ultra High Energy Cosmic Rays (UHECR) ($E_{UHECR} > 10^{19}$ eV), if their sources are known [10]. Let us assume that the distance source D is smaller than the energy attenuation length $l = E(\mathrm{d}E/\mathrm{d}r)^{-1}$ for a charged cosmic ray of energy E which can be treated constant throughout propagation. We can have two cases: the source distance is smaller than the correlation length $D \leq \lambda_B$ and the opposite $D > \lambda_B$. In the first case the deviation angle due to IGMF does not depend on the correlation length $\theta \propto Z(E_{UHECR})^{-1} B_\perp D$, where $B_\perp$ is the component of IGMF perpendicular to the line of sight and Z is the atomic charge of the cosmic ray. In the second case $D \leq \lambda_B$, as for the Faraday rotation, the angle depends on D and λ_B in the form of $\sqrt{D\lambda_B}$ so we have $\theta \propto Z(E_{UHECR})^{-1} B_\perp D^{1/2} \lambda_B^{1/2}$. Hence, in the first case knowing the distance D and energy E_{UHECR} and measuring θ would allow to estimate $B_\perp$ while in the second case one can measure the combination $B_\perp \lambda_B^{1/2}$. The ways which the cosmic rays loose their energy depend on the mass of the charged particles: for protons the main energy loss channel is pion production on Cosmic Microwave Background (CMB) while for heavy nuclei it is the photo-disintegration on cosmic infrared background. In both cases $D \sim 100$ Mpc. This is a distance limit for a source of the highest energy cosmic rays.

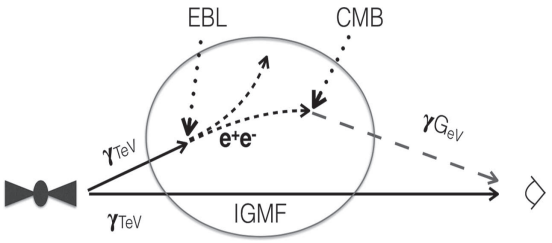

Fig. 2. – Cartoon of the reprocessing of the absorbed TeV radiation.

2˙4. *Limits from CMB anisotropy measurements.* – A magnetic field present at the decopupling ($z_d \simeq 1100$) time phase and homogeneous on scales larger than the horizon at that time, causes to the universe to expand at different rate in different directions. Since anisotropic expansion distorts the CMB, measurements of the CMB angular power spectrum permit to constrain the IGMF. Indeed, if we consider a universe homegeneus, flat and isotropic a magnetic field spatially homogeneus but unidirectional can destroy the isotropy of the Universe. Expansion along the lines of the magnetic field is inhibited by the magnetic tension and expansion in the plane perpendicular to the direction of the magnetic field is facilitated by the magnetic pressure. The net effect is that the universe expands more slowly in one direction with respect to the case in which the magnetic field is zero. In fig. 1 they are reported the limits on IGMF from CMB distortions [11-14].

3. – Limits on IGMF with γ-ray telescopes

As we can see in fig. 1 our current knowledge about IGMF is very poor. Indeed there is a huge zone of the exclusion plot which is not reachable with the standard tecnhiques. A possible new technique to improve the currents limits on IGMF involves the potential of the newly opened field of Very High Energy (VHE) γ-ray astronomy.

Multi-TeV γ-rays emitted by distant point sources are not able to propagate over long distances because they interact with the photons of the optical/infrared part of the Extragalactic Background Light (EBL) producing pairs positron and electrons ($\gamma_s + \gamma_{OPT,IR} \rightarrow e^+ + e^-$) (see fig. 2).

The mean free path of the source photons depends, obviously, on their energies and can be written as [15]

$$D_\gamma(E_{\gamma_s}, z) = 40 \frac{k}{(1+z)^2} \left[\frac{E_{\gamma_s}}{20\,\mathrm{TeV}}\right]^{-1} \mathrm{Mpc} \tag{1}$$

where $k \sim 1$ takes into account the EBL model, z is the redshift of the source and E_{γ_s} is the energy of the source photon. Hence due to the EBL the spectrum of the point source in the VHE domain will be suppressed by

$$F(E) = F(E_{\gamma_s}(z)) e^{-\tau(E_{\gamma_s}, z)}, \tag{2}$$

where $F(E)$ is the measured spectrum of the source, $F(E_{\gamma_s}(z))$ is the instrinsic spectrum and $\tau(E_{\gamma_s}, z)$ is the optical depth which depends on the energy of the TeV photon and on the distance of the source z. The produced pairs, in turn, produce secondary γ-rays

via Inverse Compton (IC) scattering on the CMB. The electrons lose their energies via IC scattering of CMB within the distance

$$D_e = 3 \times 10^{-2}(1+z_{\gamma\gamma})^{-4}\left[\frac{E_e}{10\,\mathrm{TeV}}\right]^{-1}\ \mathrm{Mpc}, \tag{3}$$

where $z_{\gamma\gamma}$ is the redshift at which the pairs are produced and E_e is the energy of the electrons. Photons emitted by the source at energies E_{γ_s} are reprocessed at energy E_γ. The relation between E_γ and E_{γ_s} is

$$E_\gamma \simeq 70\left(\frac{E_{\gamma_s}}{10\,\mathrm{TeV}}\right)^2\ \mathrm{GeV}, \tag{4}$$

photons at 10 TeV are reprocessed at 70 GeV. The amount of absorbed flux due to EBL eq. (2) is reprocessed at lower energies.

If there is a not negligible magnetic field in the IGM the pairs e^+e^-, which were initially produced in the direction of the source, could be delfected leading to two potentially observable effects:

- *spectral distortion from the secondary γ-rays.* As we explained before the primary TeV-emission from a point source is absorbed by the EBL. The final effect is that amount of the absorbed emission is reprocessed in the GeV domain. This means that measuring the absorbed emission we can predict the amount of the secondary emission. IGMF, deflecting the pairs, produces a suppression of the reprocessed emission which depends on the strength of IGMF. Comparing the expected contribution of the cascade emission with the measured spectrum it is possible to constrain the IGMF [16].
- *extended emission around a point source of γ-ray.* Since the pairs are deviated along the trajectory between the Earth and the source, the secondary emission might not be point source like but it would be in the form of an extended emission around the point source where the angular extension will be proportional to the IGMF. In order to compute the angular extension θ_{ext} of the cascade emission we need to distinguish two cases: $\lambda_B \gg D_e$ and $\lambda_B \ll D_e$. In the first case θ_{ext} does not depend on the correlation lenght $\theta_{ext} \propto (1+z)^{-2}\tau^{-1}E^{-1}B$. In the second case we get $\theta_{ext} \propto (1+z)^{-1/2}\tau^{-1}E^{-3/4}B\lambda_B^{1/2}$.

In this paper we used the MAGIC telescopes to study the possibility to detect extended emission around extragalactic TeV sources. Clearly emerges that a measurement of θ_{ext} would correspond to a measurement of the IGMF strength. A non detection would result in a limit on the IGMF.

4. – Search for extended γ-ray emission with MAGIC telescopes

MAGIC is a system of two Imaging Atmospheric Cherenkov Telescopes (IACTs) located at the Observatorio Roque de los Muchachos on the Canary Island of La Palma, Spain, which has been operating in stereoscopic mode since 2009. Prior to this, MAGIC comprised a single IACT that began operating in 2004. Most of the important characteristics of MAGIC, which are crucial for our aims, are synthesized in table I.

TABLE I. – *Main technical parameters of MAGIC telescopes* [17].

Energy threshold	$\sim 50\,\mathrm{GeV}$
Field of view	3.5°
Energy resolution	16% ($E > 300\,\mathrm{GeV}$)
Angular resolution	0.06° ($E > 300\,\mathrm{GeV}$)
Sensitivity (5σ in 50 hours)	0.8% Crab Nebula flux ($E > 250\,\mathrm{GeV}$)

Since our main goal is to detect, or at least to give an upper limit, on the extended emission around a TeV extragalacic point source, it is clear the first important step is to study the response of the instrument to a point like source. For this reason we first studied the so called Point Spread Function (PSF) of MAGIC telescopes. To carry out this study we selected a sample of data of Crab nebula because with the angular resolution of MAGIC this source can ben considered as point like.

The point-like description is then applied to the extragalactic TeV source, the blazar Markarian 421. In principle this is not the ideal source to look for an extended emission mainly for two reasons: Markarian 421 is a nearby AGN (redshift $z = 0.03$) and the expected angular extension fills or even exceeds the field of view of MAGIC making difficult to be sensitive to it. In addition because the vicinity of the source the flux expected from cascade emission is low because the optical depth τ in the eq. (2) is close to zero and then the extended emission might be very weak. However even for this surce some values of B and λ_B can be tested as previously done by MAGIC in [18], when MAGIC was operating with only one telescope. Since now MAGIC is operating in stereo mode we want to improve the upper limits on extended emission computed in [18] and then set up a procedure to detect extended emission which can be applied also to most promising sources in the next future.

In the final step we compared the two sources and computed the upper limits on extended emission.

4˙1. *Study of MAGIC PSF.* – As it was already pointed out to study the possibility to detect extended emission a deep characterization of the PSF of MAGIC is needed. To carry out this study it was selected a sample of Crab Nebula data from September 2013 to November 2013. The data sample consists in 16.8 hours in the zenith angle range 7° and 50°. The observations were performed in wobble mode [19] and the analysis has been performed using the standard MAGIC analysis chain [20, 21].

The final data sample consists of γ-like events, surviving a selection cut to discriminate γ events from the background. For each event the energy and arrival direction are estimated. With these informations it is now possible to search for a significant signal: this task is achieved with the so called θ^2 plot. θ is defined as the angular distance between the reconstructed source position and the real or assumed source position. The presence of a γ-ray source makes the distribution of θ^2, performed with respect to the nominal position of the source, peaked towards small values (see fig. 3). We built the θ^2 plot in the energy range 100–1389.5 GeV.

Once we performed the θ^2 plot of Crab we want to find an analytical description of this distribution which represents an analytical approximation of the PSF. We choose the

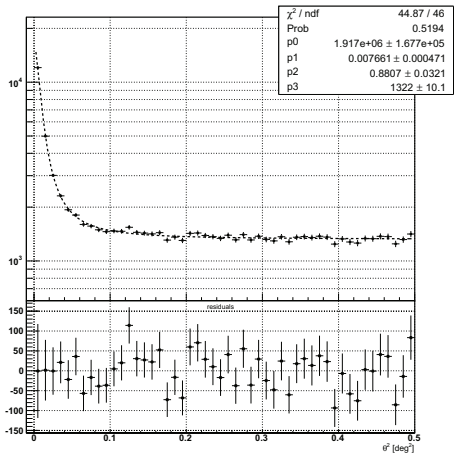

Fig. 3. – Fit of Crab θ^2 plot perfomed with the model (5). Here 1 bin = $0.01\,\mathrm{deg}^2$. In the upper panel the dashed line represents the model with the values of the parameters obtained from the fit and in the lower panel the distribution of the difference between the model and the data is plotted.

King Function [22]: this function is commonly used in X-ray experiments and recently also by FERMI Collaboration [23]. We fitted the θ^2 plot with this function:

$$\frac{\mathrm{d}N}{\mathrm{d}\theta^2} = p0 * p1 * \left[1 + \left(\frac{\theta^2}{p1}\right)^2\right]^{-p2} + p3, \tag{5}$$

where first addend is the King function and the parameter $p3$ represents the γ-like background. The parameters $p1$ and $p2$ represents the core of the King function and $p0$ is connected to the normalization and it is proportional to the integral of the King function. The fit is performed up to $0.5\,\mathrm{deg}^2$ and the results are reported in fig. 3. Visual inspection and the χ^2 show that the model (5) is a good analytical approximation of the PSF.

4˙2. *Comparison between Crab and Markarian* 421. – The function (5) represents our model of the point like source. Now we want use this model to disentangle the contribution of the point source from a possible extended emission in the source Markarian 421. First we selected a sample of data on Markarian 421 observed moreless in the same period of Crab, particularly the data go from december 2013 to april 2014. Besides the zenith range of the observations is 6°–42°. In this case we analyzed 10 hours of data. We avoided to take data during a flare beacuse in the high emission state of the source the extended component remains constant, while the point-like emission provides additional background, hence degrading the sensitivity to detect extended emission. As for Crab we produced the θ^2 plot in the same energy range 100–1389.5 GeV.

Now the main point is how to study a possible deviations of the shape of the θ^2 plot from the one of the point source, namely the Crab. Before solving this issue there is another correction we have to take into account. The spectrum of the two sources as well as the zenith distribution of the two observations can be different. This has a consequence in the shape of theta square plot and then also in the shape of the PSF.

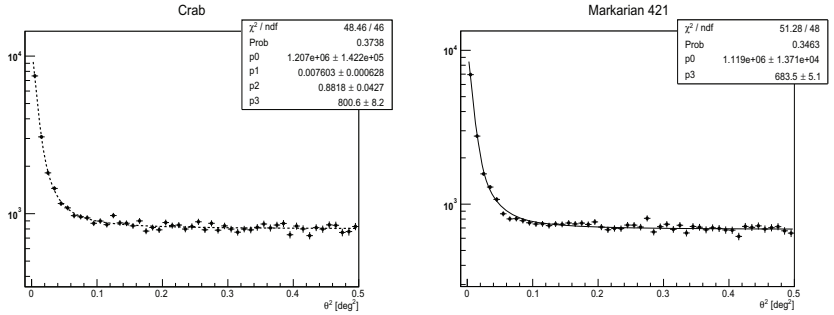

Fig. 4. – Method 1. Left panel: fit of Crab θ^2 plot with all four parameters of the fitting function (5) left free. Right panel: fit of Markarian θ^2 plot with (5) where $p1$ and $p2$ are fixed to the ones of the Crab fit.

Indeed photons at lower energies have a broader θ^2 distribution while photons with higher energies have a narrower θ^2 distribution. For this reason if the spectra of the sources are not comparable we need to rescale of the θ^2 plot of Crab to the one of Markarian before doing the comparison. In addition, since photons detected at low zentih have mainly low energies also a different shape of the zenith distribution between the two sources can influence the shape of the θ^2 plot. For this reason we rescaled the θ^2 plot of Crab to the spectrum and the zenith distribution of Markarian 421.

In order to compare the shape of the two θ^2 plot we used two independent methods:

– *method 1.* We performed the fit of the PSF-reference θ^2 plot with the four free parameters of the fitting function (5). Then we fixed p1 and p2 (which are connected to the shape of the PSF) in the θ^2 plot of Markarian 421 to the ones of the first fit. If the fit with the only parameters $p0$ and $p3$ connected to the normalization is able to describe the data, then there is no reason to claim any difference between them.

– *method 2.* We performed two independent fits with the the four free parameters of the fitting function (5). Then we produced the confidence plot of the parameters $p1$ and $p2$ with a certain significance. If the resulting contours intersect, it means that there is a region of the plane $(p1, p2)$ in which the two fitting functions can be equal, then no reason to claim any difference between them.

From fig. 4 we see that the fit of the θ^2 plot of Markarian 421 is quite good (χ^2/ndf=51.3/48 corresponding to a probability of $\sim$ 35%) and this means that this source is Crab-like. In addition from fig. 5 it clear that the two contours intersect in a wide region hence also the method 2 tells us the same thing: there is no significant statistical difference between Crab and Markarian 421.

4˙3. *Upper limits on extended emission.* – The final step is the computation of the upper limits on halo emission. In order to do this we need to assume a profile for the extended emission because in general the sensitivity for the detection of extended emission depends on the angular extension and the particular profile of the halo. We assumed a disk profile. Of course any profile we assume will be modified by the response of the instrument. The proper way to compute a profile would be to convolve the assumed model with the PSF of the instrument. In the particular case of the disk, the disk profile

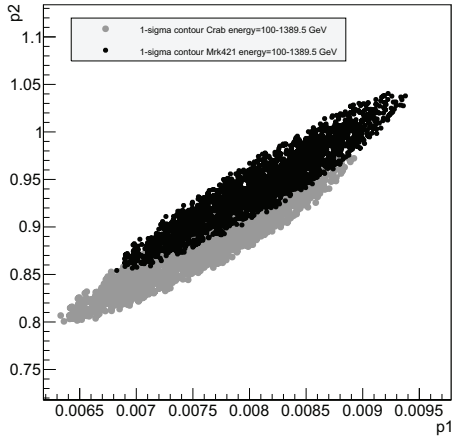

Fig. 5. – Method 2. Contour plots on the parameters $p1$ and $p2$ of the fitting function (5) at 1 sigma level performed for Crab and Markarian 421.

will be smoothed once the convolution with the King function is performed. In any case the function:

$$halo_{disk}(\theta^2) = \frac{p4}{1 + e^{k(\theta^2 - p5)}} \tag{6}$$

is a good approximation of the smoothed disk. In the model (6) the parameter $p4$ is the normalization of the disk, $p4$ is the angular extension of the halo in deg^2 and k is a constant which takes into account the shape of the tail of the disk and we fixed to 80. To be able to compare our results with the ones already published in [18] we computed the upper limits in the band 300–1300 GeV and then we reapeted the same procedure dividing the band 100–1389.5 GeV into six bins and calculating the upper limits on halo for each bin.

To compute the upper limits we produced the θ^2 plots for Markarian and Crab in the same energy band 300–1300 GeV and fitted θ^2 plot of Crab again with (5) to determine the new parameters $p1$ and $p2$ in this energy range. Then we added the model (6) to (5) fixing the parameters $p1$ and $p2$ just found in the previous fit. Now, scanning different angular extension of the halo $p5$ we repeated the fit on Markarian 421 increasing the value of the normalization of the disk $p4$ until we found a worsening of the fit with respect to the situation of no halo ($p4 = 0$) corresponding to 2σ level. Having the model of the disk and the model of the point source and knowing the fluxes of the two sources (Crab and Markarian 421) in the band 300–1300 GeV we can compute the upper limits for each angular extension in Crab units. The angular extensions we scanned are from 0.1° to 0.6°.

As we can see from the left panel of fig. 6 the most stringent upper limits is found for a disk with extension of 0.3° and it is of the order of 1.5% Crab units. In addition assuming a spectral shape of halo emission it is possible to convert the upper limit in a flux value (usually expressed in $\mathrm{TeV\,cm^{-2}\ s^{-1}}$). Assuming a power law spectrum we got that this upper limits corresponds to $4.64 \times 10^{-13}\,\mathrm{TeV\ cm^{-2}\ s^{-1}}$ and this value is plotted in the right panel of fig. 6 together with the Spectral Energy Distribution (SED) of Markarian 421. The plot in the left panel of fig. 6 can be explained in this way: for

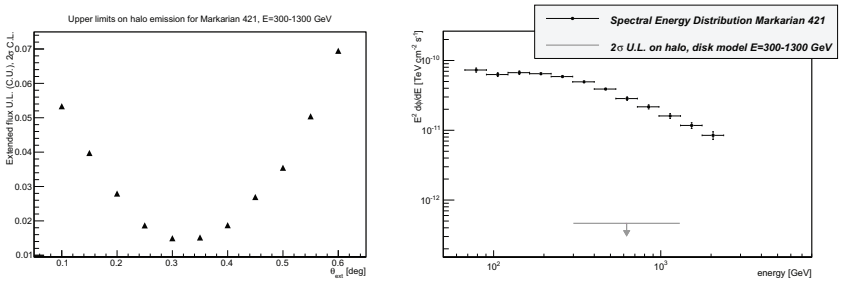

Fig. 6. – Left panel: Upper limits at 2σ in Crab units level vs halo size. Right panel: Spectral Energy Distribution of Markarian 421 and upper upper limits on halo component.

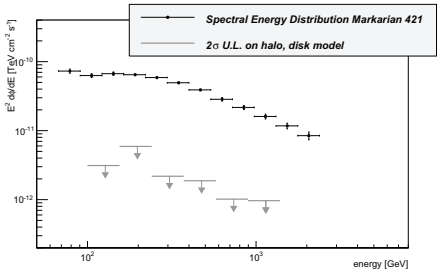

Fig. 7. – Spectral Energy Distribution of Markarian 421 and upper limits on halo emission computed in six energy bins in te range 100–1389.5 GeV.

low angular extensions the extended emission is inside the PSF and the upper limits are not stringent. When we select higher angular extensions the halo component starts to be outside the PSF and the upper limits become stringent. For really high angular extensions we are no more sensitive to detect extended emission because the halo is out of the field of view.

Finally, as anticipated above we repeated the all procedure dividing the range 100–1389.5 GeV into six bins and computing the upper limits on halo for each bin. This is possible because Markarian is a strong source and we have enough statstics in each energy bin. The results are reported in fig. 7.

5. – Discussion

In the previous section we described the procedure we used to compare the emission profile of Crab nebula and Markarian 421. Since the Markarian 421 results Crab-like we computed the upper limits on extended emission in the energy range 300–1300 GeV and 100–1389.5 GeV. In the paper [18] assuming a power law angular profile model for halo emission they found the most stringent upper limits for an angular extension of the order of 0.25°. We got an upper limit of 1.5% Crab units at 2σ level which is three times better than what obtained in [18].

The next step will be to apply this procedure to most promising sources in order to detect halo emission. Indeed as anticipated above we need sources sufficently fair way and with hard spectra such that the reproccessed emission will be strong enough to be sensitive to detect it.

REFERENCES

[1] Kronberg P. P., *Rep. Progr. Phys.*, **57** (1994) 325.
[2] Klein U., Wielebinski R. and Morsi H. W., *Astron. Astrophys.*, **190** (1988) 41.
[3] Chyży K. T. and Beck R., *Astron. Astrophys.*, **417** (2004) 541.
[4] Beck R., Fletcher A., Shukurov A. *et al.*, *Astron. Astrophys.*, **444** (2005) 739.
[5] Wolfe A. M., Jorgenson R. A., Robishaw T., Heiles C. and Prochaska J. X., *Nature*, **455** (2008) 638.
[6] Xu Y., Kronberg P. P., Habib S. and Dufton Q. W., *Astrophys. J.*, **637** (2006) 19.
[7] Kronberg P. P., Kothes R., Salter C. J. and Perillat P., *Astrophys. J.*, **659** (2007) 267.
[8] Durrer R. and Neronov A., *Astron. Astrophys.*, **21** (2013) 62.
[9] Heiles C. and Troland T. H., *Astrophys. J. Suppl.*, **151** (2004) 271.
[10] Lee S., Olinto A. V. and Sigl G., *Astrophys. J.*, **455** (1995) L21.
[11] Jedamzik K., Katalinic V. and Olinto A. V., *Phys. Rev. Lett.*, **85** (2000) 700.
[12] Barrow J. D., Ferreira P. G. and Silk J., *Phys. Rev. Lett.*, **78** (1997) 3610.
[13] Durrer R., Ferreira P. G. and Kahniashvili T., *Phys. Rev. D*, **61** (2000) 043001.
[14] Kahniashvili T., Maravin Y. and Kosowsky A., *Phys. Rev. D*, **80** (2009) 023009.
[15] Neronov A. and Semikoz D., *Phys. Rev. D*, **80** (2009) 123012.
[16] Tavecchio F., Ghisellini G., Foschini L., Bonnoli G., Ghirlanda G. and Coppi P., *Mou. Not. R. Astron. Soc.*, **406** (2010) L70.
[17] Aleksic J. *et al.*, arXiv:1409.5594 (2014).
[18] Aleksic J. *et al.*, *Astron. Astrophys.*, **524** (2010) A77.
[19] Fomin V. P., Stepanian A. A., Lamb R. C. *et al.*, *Astropart. Phys.*, **2** (1994) 137.
[20] Moralejo A. *et al.*, in *Proc. 31st ICRC (Lódź)*, arXiv:0907.0943 (2009).
[21] Lombardi S. *et al.*, in *Proc. 32nd ICRC (Beijing)*, arXiv:1109.6195 (2011).
[22] King I. R., *Publ. Astron. Soc. Pac.*, **83** (1971) 199.
[23] Ackermann M. *et al.*, *Astrophys. J.*, **765** (2013) 54.